



# Analysis of sub-daily polar motion derived from GPS with different temporal resolutions

Yaquan Peng<sup>1</sup> · Yidong Lou<sup>1</sup> · Xiaolei Dai<sup>1</sup> · Chuang Shi<sup>2</sup>

Received: 12 June 2023 / Accepted: 29 October 2023 / Published online: 17 November 2023  
© The Author(s), under exclusive licence to Springer-Verlag GmbH Germany, part of Springer Nature 2023

## Abstract

This study investigates the sub-daily polar motion (PM) derived from different estimation interval solutions ranging from 5 min/2 h. By analyzing a 3-year continuous time series of the PM estimates using Global Positioning System (GPS) observations, we conclude that PM should be parameterized as piecewise constant for intervals no longer than 30 min, while piecewise linear parameterization is more appropriate for longer intervals. The inconsistencies between the estimates and the background sub-daily PM model become more pronounced as the estimation intervals become shorter. The results demonstrate that applying continuity constraints enhances the accuracy of PM rate parameter estimation by approximately 20%. However, it is noteworthy that continuity constraints significantly modify and smooth the high-frequency content of the signal in PM. Therefore, when employing piecewise linear estimation, it is not recommended to use continuity constraints. Moreover, we find that sub-daily PM estimates are influenced by artificial signals, primarily caused by the resonance between the earth rotation and satellite revolution periods. These resonance signals are more obvious as the estimation interval becomes shorter, particularly at 4.8 and 8-h periods in the prograde and retrograde spectra, respectively. Finally, we implemented a sub-daily PM series with a 5-min temporal resolution and examined the recovery of the tidal coefficients for 38 tides. Overall, the residual signal amplitudes were generally small, with most of the main ocean tides below 5  $\mu$ s. The largest residual signals were observed for  $S_1$  and  $K_1$  terms, with amplitudes of 13.1 and 18.0  $\mu$ s, respectively.

**Keywords** GPS-based · Sub-daily polar motion · Different estimation intervals

## Introduction

Complex and multi-scale variations in the rotation of the solid earth are caused by the transfer of mass within the earth system and the exchange of angular momentum between its components (Gross et al. 2003). These variations are commonly characterized by earth orientation parameters (EOPs), which include polar motion (PM, expressed as X- and Y-pole coordinates), universal time (UT1), and the celestial pole offsets ( $dX$ ,  $dY$  representing observed corrections to the theory of precession and nutation, respectively). PM refers to the movement of the earth's spin axis around the mean pole in the earth's crust-fixed frame and the precession-nutation

is the same motion with respect to inertial space (Brzeziński et al. 2002, 2004). UT1 is solar time that represents the mean rate of the earth rotation. In addition, PM and UT1 are also known as earth rotation parameters (ERPs). Studying sub-daily variations (periods < 2 days that need sub-daily sampling) in earth's rotation contributes to a deeper scientific understanding of its dynamical system. These variations primarily arise from the redistribution and movement of mass in the solid earth, hydrosphere and atmosphere, with the hydrosphere having the most significant effect (Ray et al. 1994; Chao et al. 1996).

The current International Earth Rotation Service (IERS) convention, known as the IERS 2010 model, relies on ocean tide models derived from satellite altimetry data to predict diurnal and semidiurnal variations in PM and UT1 (Petit and Luzum 2010). In addition, the IAU2006A nutation model includes the effects of ocean tides on retrograde diurnal PM (Mathews et al. 2002). The Desai-Sibois model, based on the most recent TPX08 ocean tide model, has demonstrated superior performance in predicting sub-daily

✉ Yidong Lou  
ydlou@whu.edu.cn

<sup>1</sup> GNSS Research Center, Wuhan University, Luoyu Road 129, Wuhan 430079, Hubei, China

<sup>2</sup> School of Electronic and Information Engineering, Beihang University, Xueyuan Road 37, Beijing 100191, China

variations compared to the IERS 2010 model (Desai and Sibois 2016). However, these models do not consider the non-tidal atmosphere and ocean dynamics driven by the so-called radiational effects on sub-daily ERPs. In fact, the excitation mechanism of the atmosphere and dynamic ocean, which contribute approximately 30 and 10% to the sub-daily variations in PM and UT1, respectively, are not well understood (Gross et al. 2009). Space geodetic techniques, such as Very Long Baseline Interferometry (VLBI) and Global Navigation Satellite Systems (GNSS), are sensitive to sub-daily variations in earth rotation. PM observed from space geodetic techniques can be used to measure the disparity between background models and theoretical excitation. In theory, GNSS techniques can only observe the PM due to the strong correlation of UT1 with satellite orbital parameters. Due to its global station coverage, continuous observations and increasing precision, GNSS, in particular, has been widely used to estimate the sub-daily variations in PM.

The sub-daily PM series derived from GNSS include the combined effect of both geophysical signals and the artifacts associated with the estimation strategy. Careful handling of artificial signals is essential as they can significantly impact the geophysical interpretation of the results. Previous studies conducted by Lutz et al. (2016) and Zajdel et al. (2020) have highlighted the superiority of long-arc solutions over 1-day solutions for estimated ERPs and the improvement in noise floor by employing long-arc solutions for sub-daily PM estimation. In addition, Hefty et al. (2000) and Rothacher et al. (2001) pointed out that solar radiation pressure (SRP) modeling issues could introduce systematic effects and artificial signals into GNSS-based PM series. The utilization of a priori box-wing models mitigates spurious signals in daily PM estimation (Peng et al. 2022) and improves the amplitudes of spurious signals at the harmonics of 24 h in sub-daily estimation. Moreover, the combined multi-GNSS solution reduces spurious signals arising from the resonance between the earth rotation and the specific system satellite revolution periods (Zajdel et al. 2021).

Most studies primarily focus on improving the quality of PM estimation by enhancing orbital parameter estimation strategies, but discussions regarding sub-daily PM parameter estimation models are often overlooked. Generally, shorter update intervals are considered more suitable for capturing the full range of PM variations over time periods. A 15-min temporal resolution is currently the highest update interval estimated from GNSS observations (Sibois et al. 2017). However, it should be noted that the overlapping accuracy of the PM parameters tend to decline as the temporal resolution increase. Sibois (2011) found that the processing interval of the network solution limits the maximum frequency update of the PM estimates. When the update period of the PM parameters reaches the limit of the processing interval, the correlation between the orbital states of the GNSS satellites

and the PM parameters becomes very high, and the accuracy of the PM parameters suddenly diverges. Moreover, the continuous piecewise linear method is widely used for sub-daily PM parameter estimation when the temporal resolution is reduced to 1–2 h (Hefty et al. 2000; Englich et al. 2007; Artz et al. 2012; Rothacher et al. 2001; Zajdel et al. 2021). This parameterization establishes continuity in the parameter series by applying additional constraints, improving the accuracy of the PM estimates, especially for the rate parameters. However, the continuity constraint will smooth the signal at near 2-day periods and force some spurious signals into the daily PM estimates (Ray 2008). Similarly, undesirable side effects are expected in the sub-daily estimation when the continuity constraint is applied.

In this study, we finally provide a fully homogeneous and continuous three-year series from 2019 to 2022, with a 5-min temporal resolution of the PM from GPS observations. Our primary objective is to evaluate the impact of different estimation intervals on the recovery of signals from PM estimates and assess the quality of our PM solution with such a high temporal resolution. Therefore, observations from other GNSS constellations are not considered in our processing for the time being. We first describe our estimation strategy for generating sub-daily PM estimates based on GPS ground tracking data. Then we evaluate the PM estimates solved from different estimation intervals and conduct a significance test for the pole coordinate rate parameters. Afterward, the impact of continuity constraints on the quality of sub-daily PM is discussed in the time and frequency domains. Finally, we investigate both tidal and non-tidal signals in the time series of sub-daily PM estimates and shed light on the factors that influence the accuracy of sub-daily PM estimates.

## Estimation strategy

This section provides an overview of the methodology used to estimate sub-daily PM from GPS observations and describes the solutions adopted in this study. The calculations were performed using the Position And Navigation Data Analyst (PANDA) software (Liu et al. 2003). The sub-daily pole coordinates time series were derived from GPS observations collected by a globally distributed network of around 120 stations (as shown in Fig. 1). A network solution is adopted for precise orbit determination and sub-daily PM estimation. The processing details and the background models are summarized in Table 1. In our processing solution, the estimated parameters include station coordinates, orbital parameters (satellite position, velocities and solar radiation pressure parameters), satellite and receiver clocks, tropospheric delay and gradient parameters, ambiguities, pole coordinates and rates with sub-daily resolution, and

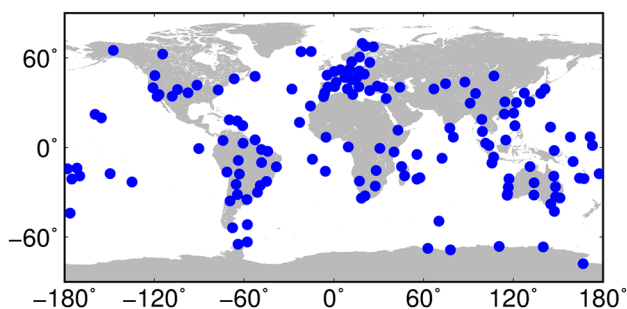


Fig. 1 Distribution of the 120 MGEX stations

pseudo-stochastic pulses. Three years of GPS data, from DOY 150, 2019 to DOY 150, 2022 are processed with a 5-min processing interval. We tested various arc lengths and found that 3-day arcs with a moving 1-day window yielded the best accuracy. We have estimated independent midpoint

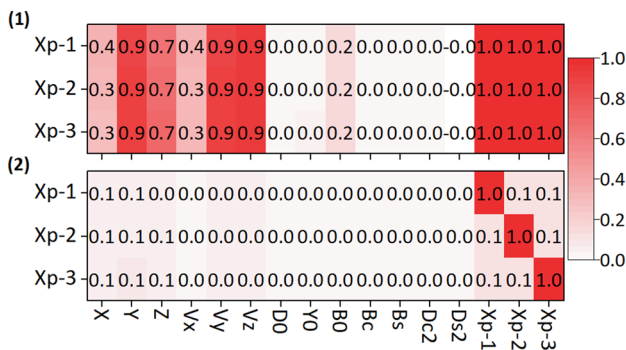
PM and rates for each interval. In addition, UT1-UTC is not estimated but is fixed to the IERS 14C04 solution. By convention, retrograde diurnal polar motion is considered pure nutation motion. Thaller et al. (2007) already described the problem of a one-to-one correlation between retrograde diurnal term of PM, nutation terms and satellite states. Nutation itself is not observable by satellite systems orbiting the earth. Therefore, the singularity between the retrograde diurnal term of PM and the orbital parameter should be resolved when dealing with sub-daily PM estimation using GPS. We use a zero-mean constraint to block the retrograde diurnal PM component, following the approach outlined by Hefty et al. (2000). The IERS provides standard pole coordinate time series, which are typically resolved daily. The lack of continuous sub-daily standard pole coordinates limits the external evaluation of our estimate. In this article, only the central daily estimates of the 3-day solution were analyzed to avoid boundary effects in our processing. In order to gain

Table 1 Description of the processing strategy

Constant processing features	Strategy
GNSS considered	GPS
Basic observables	Ionosphere-free (IF) combinations of code and phase observations. C1C/L1C and C1W/L2W for L1 band; C2L/L2L and C2W/L2W for L2 band
Code biases	corrected by the products provided by CODE
Time span	DOY 150, 2019 to DOY 150, 2022
Estimator	LSQ in batch mode
Processing interval	5-min
Arc length	3-day
A priori reference frame	IGS14 (Rebischung and Schmid 2016)
Station coordinate	Tight constraints to the igs{week}.snx ( $\sigma \leq 10^{-3}$ m)
Attitude mode	yaw-steering + eclipse attitude model (Kouba 2008; Dilssner et al. 2018; Lou et al. 2022)
Antenna phase center offsets (PCO) and variations (PCV)	igs14.atx
Antenna thrust	Rodriguez-Solano et al. (2012a)
Solar radiation pressure	ECOM2 7 parameters (Arnold et al. 2015)
Earth albedo radiation	Rodriguez-Solano et al. (2012b)
Solid earth tides, pole tides, and ocean tides	IERS 2010 (Petit and Luzum 2010); FES2014b (Lyard et al. 2021) for ocean tides
Tropospheric delay	Saastamoinen model and meteorological data from Global Pressure and Temperature (Saastamoinen 1972; Boehm et al. 2007) + Global Mapping Function (Boehm et al. 2006); Zenith wet delay and gradient parameters are parameterized as piecewise constants with a temporal resolution of 2 and 24-h, respectively
Earth orientation	Precession and Nutation: IAU2006A A priori pole coordinates: IERS 14C04 UT1-UTC: IERS 14C04 daily values (fixed) Diurnal and sub-diurnal variations: corrected by Desai-Sibois model (Desai and Sibois 2016)
Pseudo-stochastic pulses (Sigma)	Every noon and midnight epoch in the along-track ( $10^{-5}$ m/s), cross-track ( $10^{-8}$ m/s) and radial ( $10^{-6}$ m/s) directions
Variable processing features	Strategy
Pole coordinates estimate intervals	5-min/15-min/30-min/1-h/2-h
Pole coordinates estimate models	Piecewise constant/piecewise linear
Pole coordinates continuous constraint	With/without

insight into the quality of our pole coordinate estimates, we evaluate the time series through time and frequency domain analyses.

The utilization of a reasonable background model is essential for accurate sub-daily PM estimation, as highlighted by Sibois et al. (2017). In our study, the Desai-Sibois (Desai and Sibois 2016) and IERS libration (Mathews and Bretagnon 2003) models are both applied in the GPS-based pole coordinate generation process to predict the effects of the oceans and libration on sub-daily ERPs. We aimed to investigate the influence of different estimation intervals on sub-daily PM estimation. However, it is essential to discuss the modeling of PM parameters throughout the estimation interval. Table 1 summarizes the variable processing strategy in our experiment. We adopted two parameterization approaches for the PM parameter: constant and linear. This allowed us to explore the performance of PM estimates under different modeling assumptions. We employed different time intervals to investigate the impact of intervals on sub-daily PM estimation, including 5, 15, 30-min, 1 and 2-h. We observed a substantial reduction in the correlation between the satellite orbital states and PM parameters after blocking the retrograde diurnal PM. A correlation analysis when the PM parameter update period is equal to the processing interval is shown in Fig. 2. When the retrograde diurnal PM is not blocked, the position and velocity parameters of the G01 satellite exhibit a strong correlation with the pole coordinates. Similarly, a significant correlation is observed between the X-pole coordinates at different epochs. As a result, the pole coordinates cannot be accurately estimated (Sibois 2011). However, once the retrograde diurnal PM is blocked, the previously observed correlations between the pole coordinates and satellite states, and between different pole coordinates, are considerably diminished. Therefore, a 5-min temporal resolution of the PM can be estimated.



**Fig. 2** Correlations between X-pole coordinates and orbital parameters for the 5-min interval solution in DOY 150, 2019. (1) retrograde diurnal PM is not blocked (2) retrograde diurnal PM is blocked. Only the correlations between the X-pole coordinates of the first three epochs and the orbital parameters of the G01 satellite are shown for clarity

### Spectral analysis of sub-daily PM estimates

Here, in order to determine the period and amplitude of residual signals, the time series of sub-daily PM estimates were analyzed in the frequency domain. The sub-daily PM estimates were derived using both piecewise constant and linear methods, utilizing estimation intervals of 2, 1-h, 30, 15, and 5-min, respectively. We first analyzed the spectrum of the estimated PM rates. Figure 3 demonstrates the power spectra for the estimated X-pole coordinate rate series derived from the linear solution using various estimation intervals. Except for the 5 and 15-min solutions, the power spectrum shape for the X-pole coordinate rates is similar to white noise. The power spectrum of the estimated pole coordinate rates with different estimation intervals varies significantly. Shorter estimation intervals lead to increased noise in the power spectrum at high frequencies, making the estimated rates less stable and more prone to spurious signals. The power spectrum of 2, 1-h and 30-min solutions have distinct signals close to 24, 12, 8 and 6-h periods, which are attributed to various factors such as atmospheric effects, errors in background models, spurious signals from resonance between the earth rotation period and satellite revolution period and so on. The pole coordinate rates are probably useful as a probe of the geophysical excitation. However, the estimated rates are unstable and heavily contaminated by spurious signals when the estimated interval is shorter than 15-min. The source of these spurious signals is unclear, but may be due to unreliable estimates resulting from a lack of sufficient observations.

We also tested rate parameters derived from different estimation interval solutions to determine their significance. The significance of rate parameters can be determined through a general linear hypothesis test on parameters (Koch 1999; Teunissen 2000). Two hypotheses are typically postulated for rate parameters:

$$H_0 : E(\hat{v}_i) = 0 \quad \text{and} \quad H_1 : E(\hat{v}_i) = \tilde{v}_i \tag{1}$$

where  $E(\dots)$  is expectation operator; and  $\hat{v}_i$  is the estimated rate at epoch  $i$ ;  $\tilde{v}_i$  is the truth value of the rate. In our hypothesis testing, the hypothesis  $H_0$  is accepted as true. According to this assumption, the following test statistic has the  $t$ -distribution:

$$w = \frac{\hat{v}_i}{\sqrt{D_{v_i v_i}}} \sim t(n - 1) \tag{2}$$

where  $D_{v_i v_i}$  is the variance, which is obtained from the estimated covariance matrix. The test statistic  $w$  has the  $t$ -distribution with  $n - 1$  degrees of freedom, where  $n$  represents the number of estimated rates. The probability of incorrectly rejecting the hypothesis  $H_0$  is represented by the significance

**Fig. 3** Power spectrum of the estimated X-pole coordinate rate series derived from the linear solutions with different estimation intervals (Period < 2 days). The periods represented by the gray dashed lines are marked. Y-pole coordinate rates showed similar performance

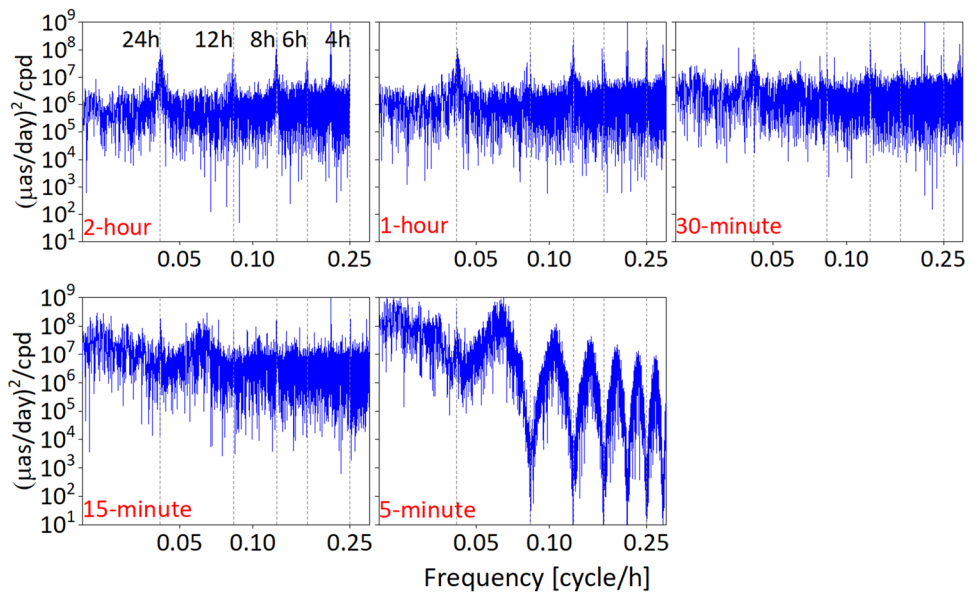


**Table 2** MSRs for the significance test with different estimation interval solutions

Estimation interval	Candidates	Accepts	MSR (%)
2-h	13,716	0	0
1-h	26,352	13,439	49
30-min	52,704	39,102	74
15-min	105,408	95,909	91
5-min	316,224	316,224	100

level ( $\alpha$ ,  $\alpha = 0.05$  in our significance test). The hypothesis  $H_0$  is accepted with a confidence level of  $1 - \alpha$  if:

$$P\left\{\left|\frac{\hat{v}_i}{\sqrt{D_{v_i v_i}}}\right| < t\left(\frac{\alpha}{2}\right)\right\} = 1 - \alpha \tag{3}$$

Then, if the test statistic  $w$  exceeds the threshold value  $t\left(\frac{\alpha}{2}\right)$ , the hypothesis is rejected with the risk of  $\alpha$ -probability. Therefore, each rate estimate  $\hat{v}_i (i = 1, 2, \dots, m)$  is individually tested using the variance  $D_{v_i v_i}$  with the test statistic in (2) at the significance level of  $\alpha = 0.05$ . The number  $k$  of the rate parameters that pass this test are counted to estimate the mean success rate (MSR) (Hekimoglu and Koch 1999):

$$MSR = \left(\frac{k}{m}\right) \times 100\% \tag{4}$$

The MSRs obtained for each estimation interval are presented in Table 2. Since we now assume that the hypothesis  $H_0$  is accepted as true, the MSRs provide the probability of correctly accepting the hypothesis  $H_0$ . As shown in Table 2, the MSRs increase gradually as the estimation

interval becomes shorter. The MSRs exceed 70% when the estimation interval does not exceed 30 min. Consequently, we assume that the rate parameters are almost negligible for estimation intervals falling within this range. In other words, the sub-daily PM should be parameterized as a piecewise constant. However, when the estimation interval is increased to 1-h, the MSR drops below 50%. When the estimation interval is 2 h, the MSR is 0%, which means that the  $H_0$  is completely rejected. Therefore, when the estimation interval exceeds 1-h, it is advisable to use the piecewise linear method for PM estimation. Furthermore, in geophysical excitation studies, using the offset values rather than the rate values would be more reliable. Figure 4 displays the difference of power spectra of the estimated X-pole coordinate series derived from the piecewise constant and piecewise linear solutions using different estimation intervals. If the constant method was incorrectly used in the 2 and 1-h estimation interval solutions, it would lead to the smoothing of the X-pole coordinate series signals. The most notable smoothing occurs around the period of 24 h. Even though the linear method is used for estimation intervals shorter than 30 min, the power spectra exhibit similar performance to the constant method series. This means that the rate parameters may have a minimal effect on the associated PM offset estimates.

We then investigate the impact of different estimation intervals on the quality of the estimated PM using this optimal method. The mean and root mean square (RMS) of the estimated PM series are presented in Table 3. The offsets for X- and Y-pole coordinates remain consistent throughout all estimation intervals, with values of 2.5 and 4.2  $\mu\text{as}$ , respectively, which are aligned with the daily solutions (Peng et al. 2022). We conclude that the estimation of sub-daily PM will

**Fig. 4** Difference of power spectrum of the estimated X-pole coordinate series derived from the linear and constant solutions with different estimation intervals (Period < 2 days). Positive values indicate that the amplitude is larger using the linear method than the constant method. The periods represented by the gray dashed lines are marked. Please note different scales for the y-axis

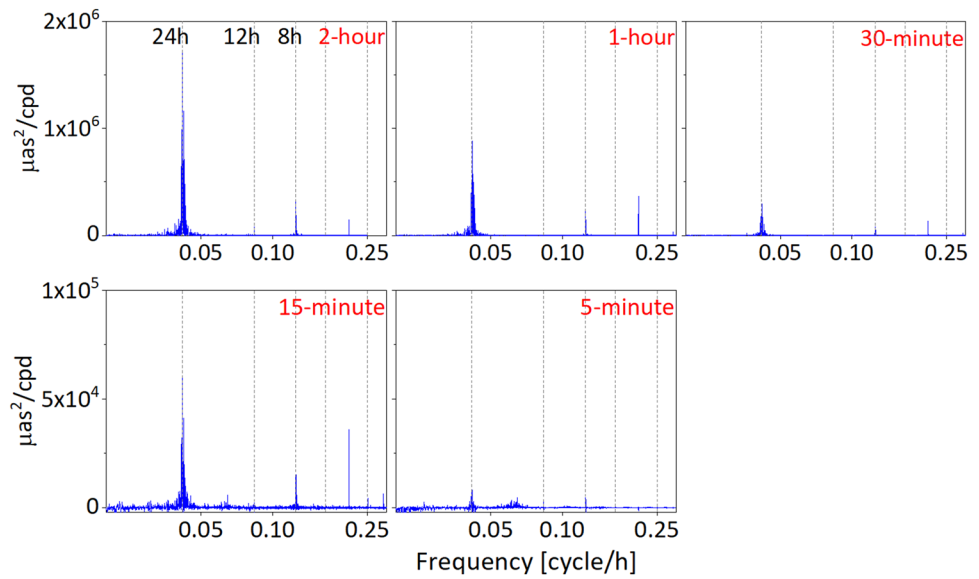


**Table 3** Statistics of the estimated PM series for different estimation interval solutions, i.e., estimated corrections with respect to the a priori model

Interval	X (µas)		Y (µas)	
	Mean	RMS	Mean	RMS
2-h	2.5	60.9	4.2	60.1
1-h	2.5	63.7	4.2	63.0
30-min	2.5	65.3	4.2	64.6
15-min	2.5	66.6	4.2	65.8
5-min	2.5	68.2	4.2	67.3

not introduce any further systematic offsets. The RMS values of X-pole (Y-pole) coordinate estimates are 60.9 (60.1), 63.7 (63.0), 65.3 (64.6), 66.6 (65.8) and 68.2 (67.3) µas for 2, 1-h, 30, 15 and 5-min solutions, respectively. The RMS of the estimated PM reflects discrepancies between the observations and the a priori values, with these inconsistencies becoming more pronounced as the estimation intervals become shorter.

### Impact of continuity constraints

The utilization of piecewise linear method is recommended when the estimation interval exceeds 1-h. Introducing continuity constraints in PM estimation can improve the stability of PM estimates, particularly for daily resolutions (Brockmann 1997). However, it is important to acknowledge that continuity constraints may also introduce artificial signals and smooth out signals in the PM estimate series. To assess the impact of continuity constraints on sub-daily PM estimation, we conducted a comparative analysis between PM

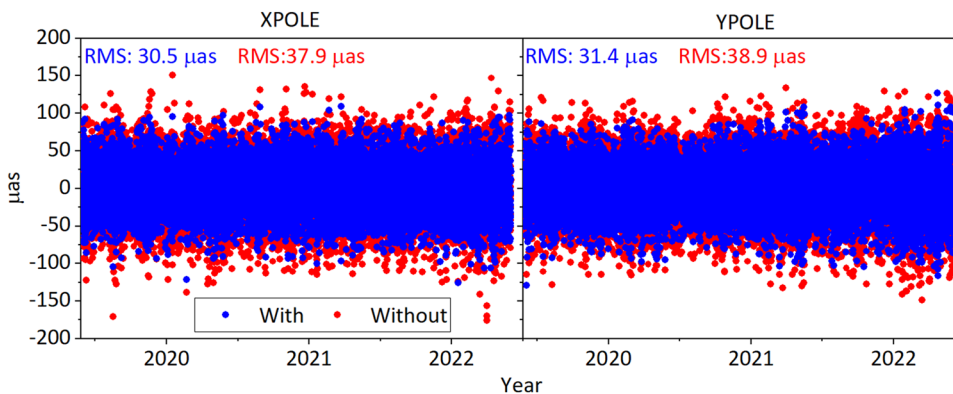
series derived from solutions with and without continuity constraints. The discontinuities of the sub-daily PM time series are presented as the differences at each estimation boundary, which can be calculated as follows:

$$Diff = [offset_2 - (0.5 * T * rate_2)] - [offset_1 + (0.5 * T * rate_1)] \tag{5}$$

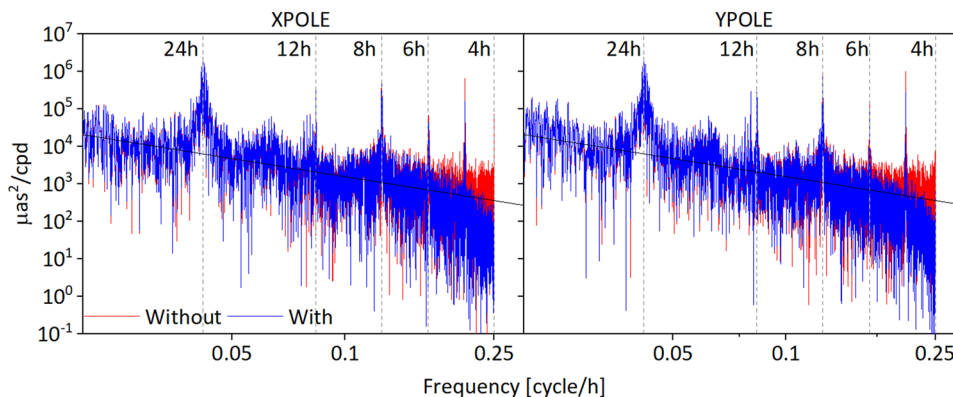
where  $offset_{12}$  and  $rate_{12}$  represent the PM and PM rate estimates for two successive intervals.  $T$  denotes the estimation interval.

Figure 5 illustrates the discontinuities in sub-daily PM estimates using a 2-h estimation interval. The corresponding RMS of these differences is also depicted in Fig. 5 for each PM component. The observed discontinuities primarily reflect the behavior of PM rate estimates. As shown, the solutions with continuity constraints exhibit reduced overall scatter. Specifically, after imposing continuity constraints, the RMS values decreased from 37.9 s to 30.5 µas for X-pole and from 38.9 to 31.4 µas for Y-pole coordinates, respectively. This represents an improvement of about 20% in RMS compared to the solutions without continuity constraints. Furthermore, Fig. 6 depicts the power spectra of the estimated PM series based on a 2-h estimation interval. For periods shorter than 2 days, the power spectra demonstrate a single power law behavior, characterized by a spectral index of approximately -1.6. However, when continuity constraints are added, the power spectra of both the X- and Y-pole coordinates gradually steepen at the highest frequencies, nearing the Nyquist limit of 0.25 cycles/h. As analysis of International GNSS Service (IGS) PM daily estimates by Ray (2008) indicated, the continuity constraint may be characterized as a peculiar phase filter that allows Nyquist-frequency signals with cosine phase aligned to the boundary to pass through but attenuates the same frequency signal

**Fig. 5** Estimated sub-daily PM discontinuities at estimation boundaries based on a 2-h estimation interval. The labels "With" and "Without" denote the solutions obtained with and without continuity constraints, respectively



**Fig. 6** Power spectrum of the estimated sub-daily PM series (Period < 2 days). A black power-law line with a spectral index of -1.6 is plotted on each plot. The periods represented by the gray dashed lines are marked. The labels "With" and "Without" denote the solutions obtained with and without continuity constraints, respectively



exactly when the phase is shifted by 90 degrees. As a result, it significantly modifies and smooths the high-frequency content of the signal, with the greatest effect, particularly at the Nyquist frequency. Compared to the independent linear parameterization, the application of continuity constraints reduces the power at the Nyquist frequency by an order of magnitude. As shown in Fig. 6, the smoothing and signal distortion effects range from 4 h to approximately 8 h. Therefore, although the continuity constraints can improve the stability of the sub-daily PM estimates, it is advisable to use the independent linear parameterization due to the potential undesirable side effects it may introduce.

**Tidal and non-tidal signals in PM variations**

Ideally, the sub-daily PM estimates should resemble white noise if all excitations have been accurately incorporated in the a priori model. However, limitations in the background model, satellite and earth revolution aliasing, and processing deficiencies may introduce spurious signals, affecting the estimates. Hence, it is important to distinguish between strategy artifacts and real geophysical signals. In this subsection, we will try to interpret the residual signals in our PM estimates and discuss the effect of different estimation

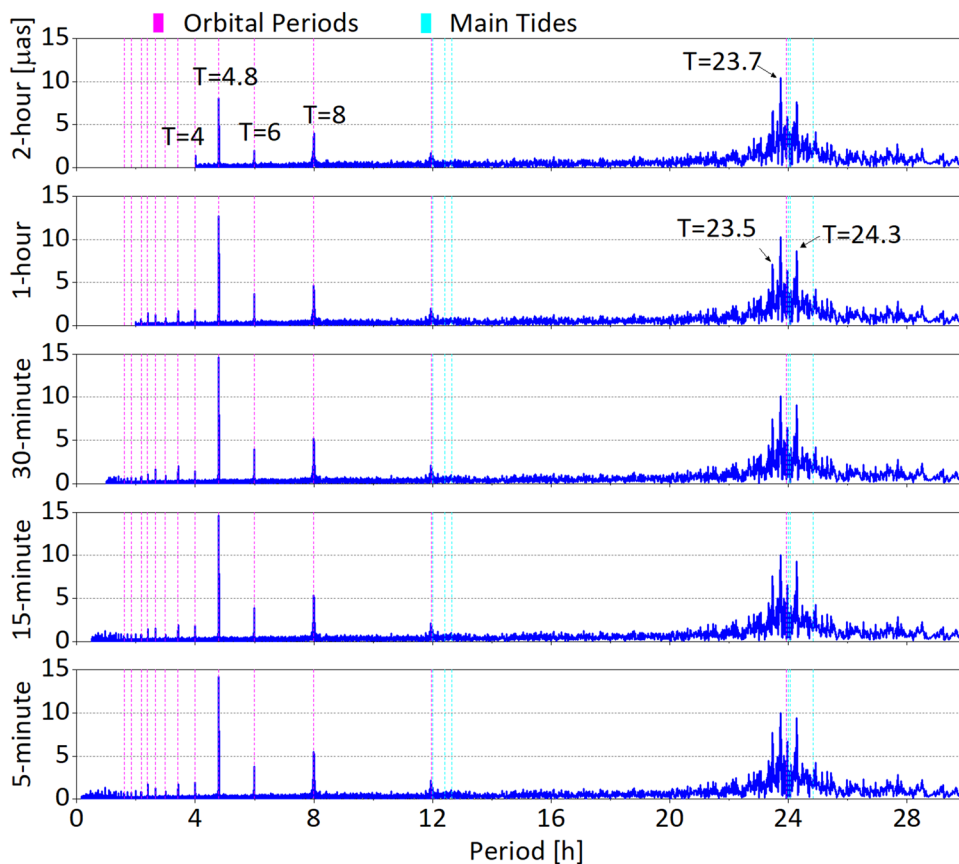
intervals on these signals. Figures 7 and 8 illustrate the spectra of the estimated PM series derived from different interval solutions, which are conventionally decomposed into prograde and retrograde directions separately. The noise floor is evaluated using the RMS of the amplitudes in the frequency domain. The noise levels in both the prograde and retrograde directions are consistently low, less than 1 μas. However, multiple signal lines are clearly observed, exceeding the noise level in both spectra. Two distinct group signals can be identified: (1) the signals at the diurnal and semidiurnal bands, which are in proximity to the theoretical periods of the main ocean tides, marked by cyan lines. (2) the signals resulting from resonance between the earth's rotation period and the satellite revolution period, denoted by magenta lines. These resonance periods can be described as (Zajdel et al. 2021):

$$P_0 = \frac{1}{n*f_s + m*f_e} \quad n, m = \{ \dots - 2, -1, 0, 1, 2, \dots \} \quad (6)$$

where  $f_s$  and  $f_e$  are the frequencies of the revolution period of the GPS satellite and of the diurnal rotation of the Earth, respectively;  $n, m$  are small integer numbers.

The first group of signals observed in our analysis may reflect the limitations of the background model for the ocean tide effects on sub-daily PM variations. The residual signals

**Fig. 7** Amplitude spectra of the estimated PM series, prograde parts for different estimation interval solutions



in the prograde spectra are more prominent in the diurnal band than the semidiurnal band. The largest discrepancies occur in the  $K_1$  tide, where the amplitude is close to 20  $\mu\text{as}$ . The retrograde PM spectra show signals with periods ranging from 20 to 28-h that approach zero, resulting from the zero constraints on blocking retrograde diurnal motion (Thaller et al. 2007). The residual signals in the semidiurnal band for the retrograde spectrum are below 5  $\mu\text{as}$ . To perform a more extensive tidal analysis, we estimated the coefficients of the sine and cosine terms of diurnal and semidiurnal variations in a constrained least-squares adjustment according to Desai and Sibois (2016). We use the estimated pole coordinates as observations and weight them by the formal errors. According to the Rayleigh’s criteria for the separation of two spectral lines, we successfully distinguished a total of 38 tidal terms from a span of 3 years data (Zajdel et al. 2021). These terms comprised 25 diurnal and 13 semidiurnal components. To accurately estimate the coefficients of the major tides, we impose constraints on the coefficient ratio between the major and their sideband tides (e.g.,  $K_1$ ,  $K_1'$  and  $K_1''$ , Gipson 1996). Subsequently, we calculated the amplitudes of the estimated PM series in each of the prograde and retrograde directions. Figure 9 illustrates the amplitudes of the estimated PM series from different interval solutions for the 9 most dominant ocean tides, labeled as

$N_2$ ,  $M_2$ ,  $S_2$ ,  $K_2$ ,  $Q_1$ ,  $O_1$ ,  $P_1$ ,  $S_1$  and  $K_1$ . A clear trend that can be observed in Fig. 9 is that the residual ocean tidal signal gets larger as the estimated interval becomes shorter. However, the difference in the amplitudes of the main ocean tides from different interval solutions is within 0.5  $\mu\text{as}$ . Thus, it can be concluded that a reasonable variation in the length of the estimation interval has a negligible influence on the recovery of the variations in PM driven by the ocean tides. To determine the accuracy and precision attainable at 5-min temporal resolution, the amplitudes and percentages of the remaining tidal signals relative to the size of the Desai-Sibois model from the 5-min estimation interval solution are shown in Table 4. The residual signal amplitudes, in general, are relatively small, typically below 5  $\mu\text{as}$  for most of the dominant tides. In addition, the percentages of the remaining tidal signals relative to the size of the Desai-Sibois model are less than 15% except for the  $S_1$  term. However, there are larger residual signals clearly visible for  $S_1$  and  $K_1$  terms, with amplitude of 13.1 and 18.0  $\mu\text{as}$ , respectively. For the  $S_1$  tidal term, most of the network parameters, such as station coordinates and orbit parameters, are estimated with a 24-h or integer multiples of the 24-h interval, which coincides with the period of  $S_1$  tide. Consequently, the discontinuity of these estimate parameters in our solutions will contribute to the signal within a period of 24 h. The  $S_1$  term is not one



**Fig. 8** Amplitude spectra of the estimated PM series, retrograde parts for different estimation interval solutions

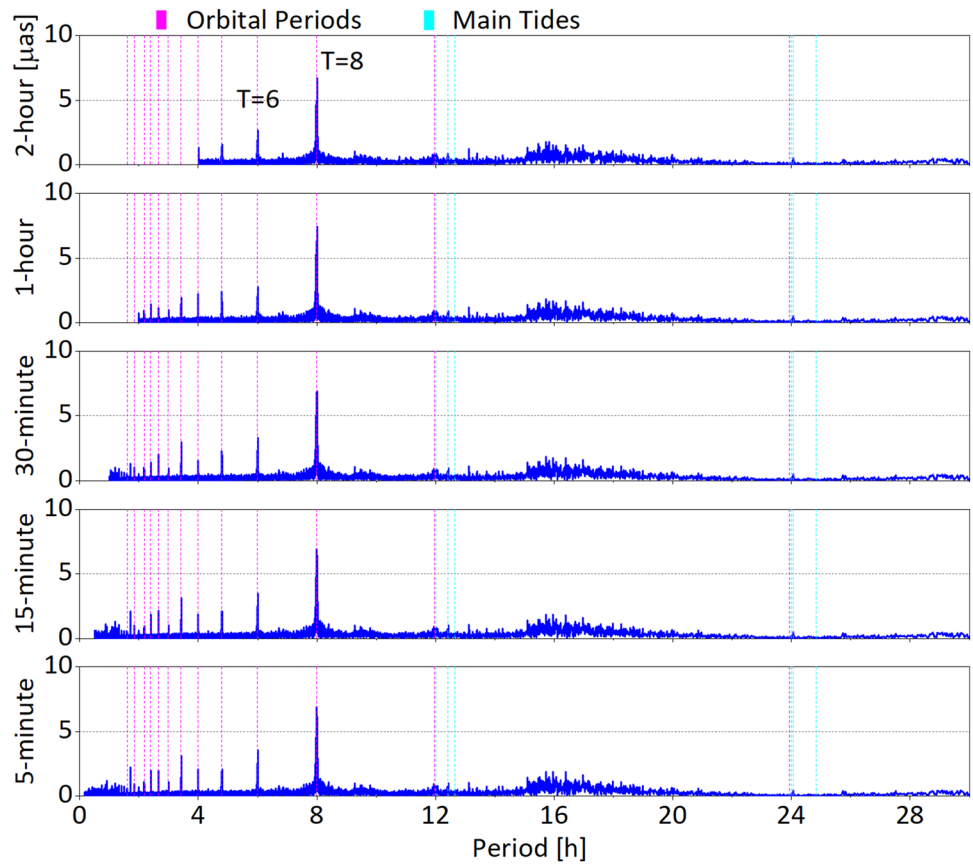


**Fig. 9** Comparison of the amplitudes for 9 main ocean tides between different interval solutions for prograde and retrograde directions

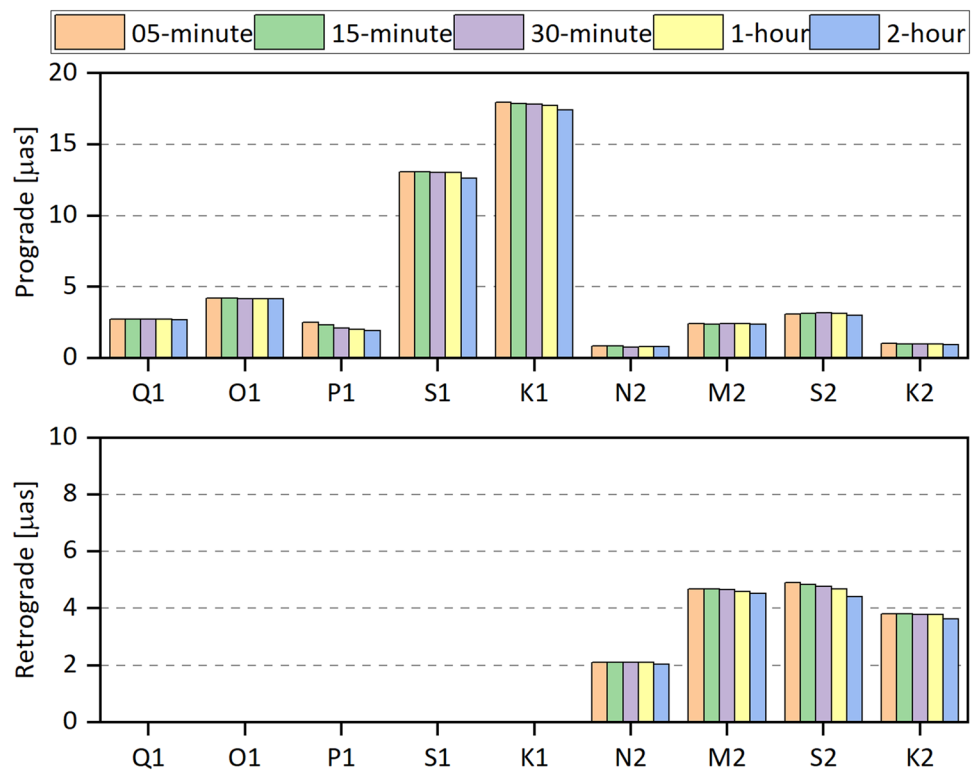


**Table 4** Amplitudes of remaining tidal signals from 5-min estimation interval solution when the Desai-Sibois model is applied and the percentages of remaining tidal signals relative to the size of the Desai-Sibois model

Tide	Prograde		Retrograde	
	Amplitude	Percentage (%)	Amplitude	Percentage (%)
$Q_1$	2.7	9.1		
$O_1$	4.2	2.9		
$P_1$	2.5	4.8		
$S_1$	13.1	1004.5		
$K_1$	18.0	10.6		
$N_2$	0.8	5.1	2.1	5.0
$M_2$	2.4	3.1	4.7	1.8
$S_2$	3.1	12.6	4.9	3.8
$K_2$	1.0	14.5	3.8	10.3

The retrograde diurnal signals are not estimated. Units are  $\mu\text{s}$

of the main tidal terms and has an amplitude of only 1.3  $\mu\text{s}$  in the Desai-Sibois model. Thus, the remaining percentage of the  $S_1$  tide is up to 1004.5% in Table 4. As for the  $K_1$  tidal term, it is worth noting that the repeat period of the GPS constellation, which lasts approximately 23 h and 56 min, coincides with the period of  $K_1$  tide. As a result, the resonance signal is expected to alias into the sub-daily PM estimated specifically for the  $K_1$  tide. Furthermore, the residual signals exhibit prograde diurnal amplitudes of 18.0, 2.5, 4.2 and 2.7  $\mu\text{s}$  for  $K_1$ ,  $P_1$ ,  $O_1$  and  $Q_1$ , respectively. The semidiurnal amplitudes in the prograde and retrograde components are as follows: 1.0 and 3.8  $\mu\text{s}$  for  $K_2$ , 3.1 and 4.9  $\mu\text{s}$  for  $S_2$ , 2.4 and 4.7  $\mu\text{s}$  for  $M_2$ , and 0.8 and 2.1  $\mu\text{s}$  for  $N_2$ , respectively. Notably, the amplitudes of the residual signals listed in Table 4 are comparable to the results reported by Sibois (2019).

The second group is caused by the resonance between the earth rotation period and the satellites resolution period, which is not a true geophysical signal. As shown in Figs. 7 and 8, the magenta lines match well for most of these spurious signals. The amplitude of the most pronounced resonant signal in the prograde spectra, at a period of 4.8-h, is 9.4, 13.7, 13.9, 14.0 and 14.0  $\mu\text{s}$  for 2, 1-h, 30, 15 and 5-min solutions, respectively. In the retrograde spectra, a clear signal is observed at 8 h, with amplitudes of 6.4, 6.8, 6.9, 7.0 and 7.0  $\mu\text{s}$  for the corresponding interval solutions. Therefore, we can infer that as the estimation interval becomes shorter, the resonance signals become more pronounced. In fact, sub-daily variations at 6, 8, 12, 24 h are also partly attributed to atmospheric tides and non-tidal atmosphere, dynamic ocean, and continental hydrosphere angular momenta (de Viron et al. 2005). However, accurately distinguishing and measuring the individual contributions of these factors remains a challenge, as we can only observe

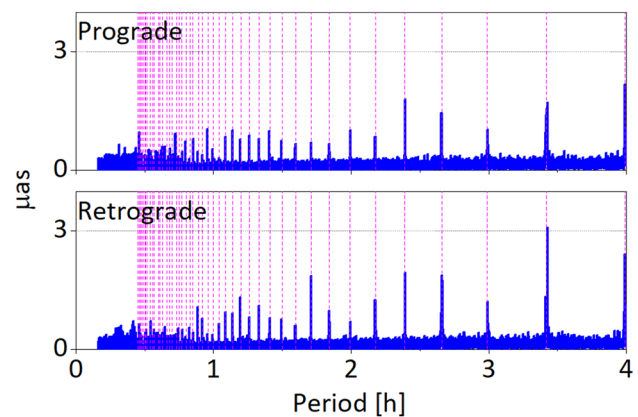


**Fig. 10** Amplitude spectra of the estimated PM series derived from 5-min estimation interval solution, prograde and retrograde parts for periods < 4 h

the combined effects. Additionally, signals are visible at the periods of 23.46, 23.73 and 24.26 h, none of which belong to any group mentioned above. There is even a peak of about 10  $\mu\text{s}$  at the period of 23.73-h. These signals may be derived from some deficiencies in our processing approach. To investigate the residual signals within the periods of 4-h, the prograde and retrograde spectra for periods less than 4 h are plotted in Fig. 10. It is observed that the amplitudes of many visible signals exceed 1  $\mu\text{s}$ , with a maximum of 3  $\mu\text{s}$ . At first sight, all visible signals can be attributed to resonance signals. However, it is crucial to acknowledge that the periods of actual geophysical signals may also align with resonance periods. Therefore, additional theoretical support is necessary to substantiate our results.

## Conclusion

The GNSS technique can be used for the recovery of the pole coordinates with a sub-daily resolution. We investigate the impact of different estimation intervals on GPS-based sub-daily PM estimation. Initially, a significance test is performed on the sub-daily pole coordinate rates, revealing that the rate parameters are almost negligible for estimation intervals that do not exceed 30 min. Consequently, PM should be parameterized as piecewise constant for intervals no more than 30 min and as piecewise linear for longer intervals. It is worth noting that the rate parameters have a minimal effect on the associated PM offset estimates. The RMS of the estimated PM series increases as the estimation intervals become shorter.

Moreover, the continuity constraints can enhance the PM rate parameter estimation accuracy by approximately 20%. However, the continuity constraints act as a peculiar phase filter. It passes signals at Nyquist frequency with the cosine

phase aligned to the boundary while attenuating the same frequency signal exactly when the phase is shifted by 90 degrees. As a result, the continuity constraints significantly modify and smooth the high-frequency content of the signal, with the greatest effect, particularly at the Nyquist frequency. Therefore, although the continuity constraints can improve the stability of the sub-daily PM estimates, it is advisable to use the independent linear parameterization due to the potential undesirable side effects it may introduce.

Furthermore, two groups of signals can be identified in the estimated PM series. The first group is the signals at the diurnal and semidiurnal bands, which are proximate to the theoretical periods of main ocean tides. The second group results from resonance between the earth's rotation and satellite revolution periods. We found no significant difference in the residual signals at the diurnal and semidiurnal bands close to the ocean tidal constituents between different interval solutions. We estimated coefficients for all 38 tidal terms using the 5-min estimated PM series. The residual signal amplitudes generally are below 5  $\mu\text{s}$  for most the dominant tides. The largest residual signals were observed for S1 and K1 terms, with amplitudes of 13.1 and 18.0  $\mu\text{s}$ , respectively. In addition, the resonance signals become more pronounced as the estimation interval becomes shorter, particularly at 4.8 and 8-h periods in the prograde and retrograde spectra, respectively. Although the resonance signals can explain most of the residual signals, accurately separating the true variation at 6, 8, 12, and 24-h caused by atmospheric tides and dynamic ocean remains challenging. Finally, we also discuss the residual signals within the period of 4-h. However, as the periods of actual geophysical signals may align with resonance periods, we need more theoretical support to substantiate our results. On the other hand, the impact of the spurious signals in the frequency domain shows a notable decrease in the combined multi-GNSS solution (Zajdel et al. 2021). However, the contribution of the BeiDou constellation was not mentioned. The observation period of most BeiDou satellites is close to 3 years. Adding BeiDou observations to the sub-daily PM estimation may decorrelate and attenuate some of the spurious signals, which needs further investigation.

**Acknowledgements** Thanks for the data support of IGS and IERS. This study is supported by the National Natural Science Foundation of China (41931075, 42374033) and the Key Research and Development Program of Hubei Province (No. 2022BAA054). The numerical calculations in this paper have been done on the supercomputing system in the Supercomputing Center of Wuhan University. Finally, we thank Prof. Aleksander Brzeziński and the anonymous reviewers for the thorough review and constructive comments that improved quality.

**Author contributions** YP and XD wrote the main manuscript text. All authors reviewed the manuscript.

**Data availability** The GNSS data of MGEX are provided by the IGS and can be accessed through <https://cddis.nasa.gov>.

## Declarations

**Conflict of interest** The authors declare no competing interests.

## References

- Arnold D, Meindl M, Beutler G, Dach R, Schaer S, Lutz S, Prange L, Sošnica K, Mervart L, Jäggi A (2015) CODE's new solar radiation pressure model for GNSS orbit determination. *J Geod* 89(8):775–791. <https://doi.org/10.1007/s00190-015-0814-4>
- Artz T, Bernhard L, Nothnagel A, Steigenberger P, Tesmer S (2012) Methodology for the combination of sub-daily Earth rotation from GPS and VLBI observations. *J Geod* 86(3):221–239. <https://doi.org/10.1007/s00190-011-0512-9>
- Boehm J, Niell A, Tregoning P, Schuh H (2006) Global Mapping Function (GMF): a new empirical mapping function based on numerical weather model data. *Geophys Res Lett* 33(7):L07304. <https://doi.org/10.1029/2005GL025554>
- Boehm J, Heinkelmann R, Schuh H (2007) Short note: a global model of pressure and temperature for geodetic applications. *J Geod* 81(10):679–683. <https://doi.org/10.1007/s00190-007-0135-3>
- Brockmann E (1997) Combination of solution for geodetic and geodynamic applications of the Global Positioning System (GPS). PhD thesis, Swiss Geodetic Commission, Zurich. <https://www.sgc.ethz.ch/sgc-volumes/sgk-55.pdf>
- Brzeziński A, Bizouard C, Petrov S (2002) Influence of the atmosphere on earth rotation: What new can be learned from the recent atmospheric angular momentum estimates? *Surv Geophys* 23(1):33–69. <https://doi.org/10.1023/A:1014847319391>
- Brzeziński A, Ponte R, Ali A (2004) Nontidal oceanic excitation of nutation and diurnal/semidiurnal polar motion revisited. *J Geophys Res Solid Earth* 109:B11407. <https://doi.org/10.1029/2004JB003054>
- Chao B, Ray R, Gipson J, Egbert G, Ma C (1996) Diurnal/semidiurnal polar motion excited by oceanic tidal angular momentum. *J Geophys Res* 101(B9):20151–20163. <https://doi.org/10.1029/96JB01649>
- Petit G, Luzum B (eds) IERS Conventions (2010) Frankfurt am main: Verlag des Bundesamts für Kartographie und Geodäsie, 179pp. ISBN 3–89888–989–6. [https://iers-conventions.obspm.fr/conventions\\_versions.php](https://iers-conventions.obspm.fr/conventions_versions.php)
- Desai S, Sibois A (2016) Evaluating predicted diurnal and semidiurnal tidal variations in polar motion with GPS-based observations. *J Geophys Res Solid Earth* 121(7):5237–5256. <https://doi.org/10.1002/2016JB013125>
- deViron O, Schwarbaum G, Lott F, Dehant V (2005) Diurnal and sub-diurnal effects of the atmosphere on the Earth rotation and geocenter motion. *J Geophys Res* 110:B11. <https://doi.org/10.1029/2005JB003761>
- Dilssner F, Laufer G, Springer T, Schönemann E, Enderle W (2018) The BeiDou attitude model for continuous yawing MEO and IGSO spacecraft. EGU 2018, Vienna. [http://navigation-office.esa.int/attachments\\_29393052\\_1\\_EGU2018\\_Dilssner\\_Final.pdf](http://navigation-office.esa.int/attachments_29393052_1_EGU2018_Dilssner_Final.pdf)
- Englich S, Mendes-Cerveira PJ, Weber R, Schuh H (2007) Determination of Earth rotation variations by means of VLBI and GPS and comparison to conventional models. *Vermess Geoinf* 2:104–112. [https://www.erdrotation.de/publication\\_p08\\_englich\\_vgi2007\\_003.pdf](https://www.erdrotation.de/publication_p08_englich_vgi2007_003.pdf)
- Gipson J (1996) Very long baseline interferometry determination of neglected tidal terms in high-frequency Earth orientation variation. *J Geophys Res Solid Earth* 101(B12):28051–28064. <https://doi.org/10.1029/96JB02292>

- Gross R, Fukumori I, Menemenlis D (2003) Atmospheric and oceanic excitation of the Earth's wobbles during 1980–2000. *J Geophys Res* 108(B8):2370. <https://doi.org/10.1029/2002JB002143>
- Gross R, Beutler G, Plag H (2009) Integrated scientific and societal user requirements and functional specifications for the GGOS. In: *Global geodetic observing system*. Springer, Berlin. [https://doi.org/10.1007/978-3-642-02687-4\\_7](https://doi.org/10.1007/978-3-642-02687-4_7)
- Hefty J, Rothacher M, Springer T, Weber R, Beutler G (2000) Analysis of the first year of Earth rotation parameters with a sub-daily resolution gained at the CODE processing center of the IGS. *J Geod* 74(6):479–487. <https://doi.org/10.1007/s001900000108>
- Hekimoglu, S, and Koch, K (1999) How can reliability of robust methods be measured? In: Altan, Gruending (eds) 3rd Turkish-German joint geodetic days. Towards a digital age, vol 1. Istanbul Technical University, Istanbul, pp 179–196
- Koch, K (1999) Parameter estimation and hypothesis testing in linear models. Springer, Berlin. <https://doi.org/10.1007/978-3-662-03976-2>
- Kouba J (2008) A simplified yaw-attitude model for eclipsing GPS satellites. *GPS Solut* 13(1):1–12. <https://doi.org/10.1007/s10291-008-0092-1>
- Liu J, Ge M (2003) PANDA software and its preliminary result of positioning and orbit determination. *Wuhan Univ J Nat Sci* 8:603–609. <https://doi.org/10.1007/BF02899825>
- Lou Y, Dai X, Gong X, Li C, Qing Y, Liu Y, Peng Y, Gu S (2022) A review of real-time multi-GNSS precise orbit determination based on the filter method. *Satell Navig* 3(1):15. <https://doi.org/10.1186/s43020-022-00075-1>
- Lutz S, Meindl M, Steigenberger P, Beutler G, Sošnica K, Schaer S, Dach R, Arnold D, Thaller D, Jaggi A (2016) Impact of the arc length on GNSS analysis results. *J Geod* 90(4):365–378. <https://doi.org/10.1007/s00190-015-0878-1>
- Lyard F, Allain D, Cancet M, Carrère L, Picot N (2021) FES2014 global ocean tide atlas: design and performance. *Ocean Sci* 17(3):615–649. <https://doi.org/10.5194/os-17-615-2021>
- Mathews P, Bretagnon P (2003) Polar motions equivalent to high frequency nutations for a nonrigid Earth with anelastic mantle. *Astron Astrophys* 400(3):1113–1128. <https://doi.org/10.1051/0004-6361:20021795>
- Mathews P, Herring T, Buffett B (2002) Modeling of nutation and precession: new nutation series for nonrigid Earth and insights into the Earth's interior. *J Geophys Res Solid Earth*. <https://doi.org/10.1029/2001JB000390>
- Peng Y, Lou Y, Dai X, Guo J, Shi C (2022) Impact of radiation pressure models on earth rotation parameters derived from BDS. *GPS Solut* 26(4):126. <https://doi.org/10.1007/s10291-022-01316-1>
- Ray J (2008) Analysis effects in IGS polar motion estimates. <http://acc.igs.org/erp-index.html>. Accessed 21 Mar 2023
- Ray R, Steinberg D, Chao B, Cartwright D (1994) Diurnal and semi-diurnal variations in the Earth's rotation rate induced by oceanic tides. *Science* 264(5160):830–832. <https://doi.org/10.1126/science.264.5160.830>
- Rebischung P, Schmid R (2016) IGS14/igs14.atx: a new framework for the IGS products. American Geophysical Union Fall Meeting 2016 San Francisco. <https://mediatum.ub.tum.de/doc/1341338/file.pdf>
- Rodriguez-Solano C, Hugentobler U, Steigenberger P (2012a) Adjustable box-wing model for solar radiation pressure impacting GPS satellites. *Adv Space Res* 49(7):1113–1128. <https://doi.org/10.1016/j.asr.2012.01.016>
- Rodriguez-Solano C, Hugentobler U, Steigenberger P, Lutz S (2012b) Impact of Earth radiation pressure on GPS position estimates. *J Geod* 86(5):309–317. <https://doi.org/10.1007/s00190-011-0517-4>
- Rothacher M, Beutler G, Weber R, Hefty J (2001) High-frequency variations in Earth rotation from Global Positioning System data. *J Geophys Res Solid Earth* 106(B7):13711–13738. <https://doi.org/10.1029/2000JB900393>
- Saastamoinen J (1972) Contribution to the theory of atmospheric refraction. *B Geod* 105(1):279–298. <https://doi.org/10.1007/BF02521844>
- Sibois A (2011) GPS-based sub-hourly polar motion estimates: strategies and applications. PhD thesis, University of Colorado, Boulder. <https://scholar.colorado.edu/downloads/pk02c9902>
- Sibois A (2019) Analysis of high-frequency EOP (HFEO) models and their impact on GPS data processing. IGS ACC Workshop, April 2019, Potsdam. [https://s3-ap-southeast-2.amazonaws.com/igs-acc-web/igs-acc-website/workshop2019/Sibois\\_IgsAcWorksop\\_2019.pdf](https://s3-ap-southeast-2.amazonaws.com/igs-acc-web/igs-acc-website/workshop2019/Sibois_IgsAcWorksop_2019.pdf)
- Sibois A, Desai S, Bertiger W, Haines B (2017) Analysis of decadelong time series of GPS-based polar motion estimates at 15-min temporal resolution. *J Geod* 91(8):965–983. <https://doi.org/10.1007/s00190-017-1001-6>
- Teunissen P (2000) Testing theory an introduction. Delft University Press Delft, 156p. ISBN 978-9040719752
- Thaller D, Krügel M, Rothacher M, Tesmer V, Schmid R, Angermann D (2007) Combined Earth orientation parameters based on homogeneous and continuous VLBI and GPS data. *J Geod* 81(6–8):529–541. <https://doi.org/10.1007/s00190-006-0115-z>
- Zajdel R, Sošnica K, Bury G, Dach R, Prange L (2020) System-specific systematic errors in earth rotation parameters derived from GPS, GLONASS, and Galileo. *GPS Solut*. <https://doi.org/10.1007/s10291-020-00989-w>
- Zajdel R, Sošnica K, Bury G, Dach R, Prange L, Kazmierski K (2021) Sub-daily polar motion from GPS, GLONASS, and Galileo. *J Geod* 95(1):3. <https://doi.org/10.1007/s00190-020-01453-w>

**Publisher's Note** Springer Nature remains neutral with regard to jurisdictional claims in published maps and institutional affiliations.

Springer Nature or its licensor (e.g. a society or other partner) holds exclusive rights to this article under a publishing agreement with the author(s) or other rightsholder(s); author self-archiving of the accepted manuscript version of this article is solely governed by the terms of such publishing agreement and applicable law.



**Yaquan Peng** is a Ph.D. candidate at GNSS Research Center, Wuhan University. His current research mainly focuses on precise orbit determination and its application for geosciences.



**Yidong Lou** received his Ph.D. in Geodesy and Surveying Engineering from Wuhan University in 2008, and is a professor at GNSS Research Center, Wuhan University. His current research interest is in real-time precise GNSS orbit determination and real-time GNSS PPP.



**Chuang Shi** is currently a professor at the Research Institute for Frontier Science, Beihang University. He graduated from the Wuhan Institute of Surveying and Mapping (currently Wuhan University) and obtained his Ph.D. in 1998. His research interests include network adjustment, precise orbit determination for GNSS satellites and LEOs, as well as real-time PPP.



**Xiaolei Dai** is currently an associate professor at Wuhan University. She received her Ph.D. degree from Wuhan University in 2016. Her current research interests are real-time precise orbit determination and clock estimation of GNSS, orbit attitude and force modeling for BDS and real-time data processing in the RTS system.